Design and Implementation of a Broadband (2 GHz – 112 GHz) Ferromagnetic Resonance Spectrometer

Daniel B. Gopman and Jenae E. Shoup, Materials Science and Engineering Division, NIST

December 3, 2025

NIST CHIPS Metrology Program *High Speed Metrology of Magnetoelectronic Devices and Models*

NIST NATIONAL INSTITUTE OF STANDARDS AND TECHNOLOGY
U.S. DEPARTMENT OF COMMERCE

Executive Summary

As spintronic devices scale down, the materials required—specifically those with high perpendicular magnetic anisotropy (PMA)—demand characterization tools that exceed the capabilities of standard commercial systems [1]. This white paper outlines the construction of a custom broadband Ferromagnetic Resonance (FMR) spectrometer capable of generating radio-frequency excitation over a continuous range from 2 GHz up to 112 GHz. By utilizing a multi-band grounded coplanar waveguide (GCPWG) architecture, off-the-shelf microwave components, and open-source software control, laboratories can replicate this system to accurately measure Heisenberg exchange stiffness and high-frequency spin-wave dynamics in next-generation magnetic films.

Table of Contents

1. Motivation: Bridging the Frequency Gap

The development of high-density magnetic random-access memory (MRAM) relies heavily on materials like $L1_0$ —ordered FePd, FePt and Mn-based Heusler alloys, which exhibit high retention stability due to bulk magnetocrystalline anisotropy. However, characterizing these materials presents significant metrology challenges:

- **The "Dead Zone":** Standard stripline FMR tools typically cap at (40–50) GHz. Conversely, optical pump-probe techniques can reach THz frequencies but often lack the required spectral resolution for fine structure analysis.
- **High-Frequency Requirements:** For films with moderate exchange stiffness ($A_{ex} \approx 10^{-11}\mathrm{J/m}$) and typical bit cell thicknesses ($10^{-9}\mathrm{m}$), the perpendicular standing spin-wave (PSSW) modes are pushed into the THz range [2].
- **Resolution of Modes:** To resolve the critical splitting between the fundamental ($n = 0$) and first order ($n = 1$) PSSW modes in thicker films (20 nm – 50 nm), researchers require high-fidelity signal detection in the 40 GHz – 110 GHz window. As demonstrated in Figure 1, the spectrometer successfully captures the linear dispersion characteristic of perpendicular ferromagnetic resonance (FMR) up to 112 GHz. The data, taken from a 47-nm-thick $L1_0$ Fe-Pd film [1], follows the Kittel relationship for a film saturated perpendicular to the plane [3[4]]:

  $$f = \gamma\mu_0\left(H_{res} + H_{k,eff} + H_{ex}\right),$$

  where γ is the gyromagnetic ratio and $H_{k,eff}$ is the effective anisotropy field. The system's high frequency resolution allows for the distinct separation of the fundamental ($n = 0$) and exchange-dominated ($n = 1$) spin-wave modes.

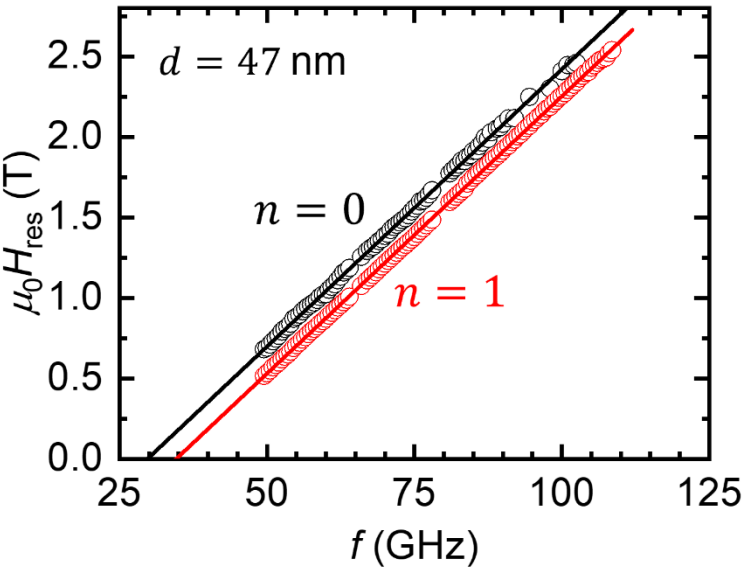

Figure 1: Broadband FMR response of a 47-nm-thick $L1_0$ Fe-Pd film with perpendicular magnetic anisotropy. The data maps the resonance frequency (f) against the external field (H_{res}) from 40 GHz to >110 GHz. The linear dispersion follows the Kittel relationship for thin-film FMR under an out-of-plane applied external magnetic field. The plot resolves the splitting between the uniform mode ($n = 0$, black) and the first standing spin-wave mode ($n = 1$, red), as detailed in Ref. [1].

2. System Architecture

The spectrometer achieves its ultra-wide bandwidth by splitting the signal generation across three distinct frequency bands, all integrated into a single probe assembly.

2.1 Microwave Signal Generation

The system eschews exotic, singular wideband sources in favor of three independent microwave generators coupled with amplified frequency multipliers to achieve 112 GHz.

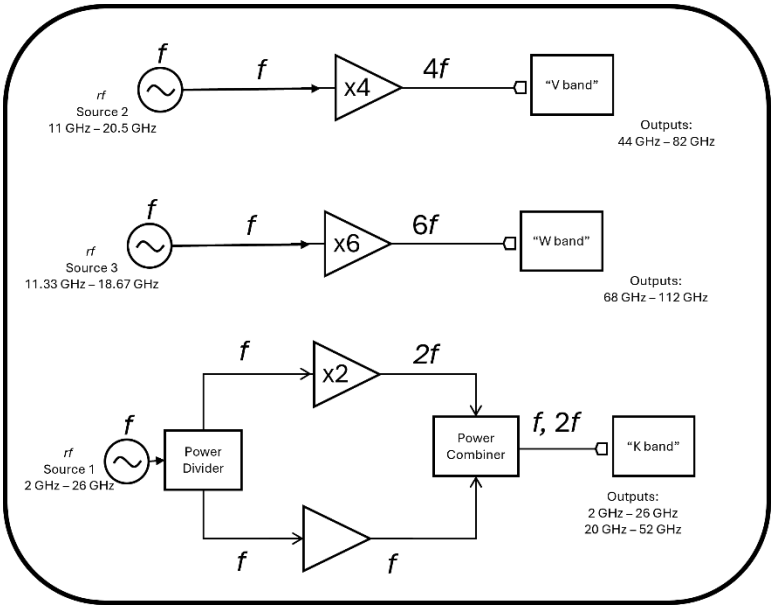

Figure 2: Circuit schematic highlighting amplification and frequency multiplication circuitry used to deliver continuous-wave rf signals spanning 2 GHz—112 GHz.

- **K Band (2–52 GHz):**
    - *Source:* Generator 1 (2 GHz—26 GHz).
    - *Path:* A resistive power divider splits the signal. One path feeds a standard broadband amplifier (0.3 GHz—35 GHz). The other feeds a frequency-doubling amplifier (x2) to cover 20 GHz—52 GHz. These signals are recombined to feed the low-frequency line.
- **V Band (44–82 GHz):**
    - *Source:* Generator 2 (11 GHz—20.5 GHz).
    - *Multiplier:* An x4 active frequency multiplier converts the input to 44 GHz—82 GHz, delivering a nominal 16 dBm output power (50 GHz—75 GHz).
- **W Band (68–112 GHz):**
    - *Source:* Generator 3 (11.33 GHz—18.67 GHz).
    - *Multiplier:* An x6 active frequency multiplier converts the input to 68 GHz—112 GHz, delivering 16 dBm output power (75 GHz—105 GHz).

3. The Probe: Custom GCPWG Board Design

The core innovation of the system is the sample probe—a custom dielectric board designed to minimize radiative losses while maintaining impedance matching across the frequency spectrum.

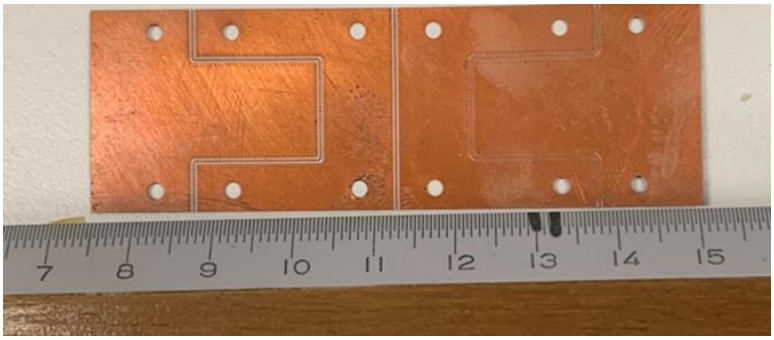

Figure 3: Custom GCPWG board fabricated on Rogers 4350 dielectric, featuring three transmission lines optimized for K, V, and W bands.

3.1 Board Specifications

- **Substrate Material: Rogers 4350** dielectric laminate.
- **Dimensions:** 0.20 mm (8 mils) dielectric thickness with a relative permittivity of $\epsilon_r = 3.2$. The board is coated with 0.025 mm (2 mils) of Copper on each side.
- **Transmission Lines:** Three lines run parallel along the board. To minimize magnetic field gradients at the sample location, the lines narrow from a separation of 25.4 mm at the connectors to 9.53 mm at the center.

3.2 Signal Integrity Engineering

To support frequencies up to 112 GHz, the board layout addresses inductance and radiation:

- **Inductance Compensation:** A 1-mm-long taper transitions the trace width from 0.13 mm (5 mils) at the connector edge to 0.25 mm (10 mils) on the board. This mitigates the parasitic inductance introduced by the 1.0 mm connector pins [5].
- **Radiative Loss Suppression:** Metallized vias (0.13 mm diameter) connect the top and bottom ground planes. A critical edge-to-edge spacing of 0.15 mm ensures separation is less than $\lambda/8$ at 120 GHz (0.18 mm), effectively suppressing radiative losses.

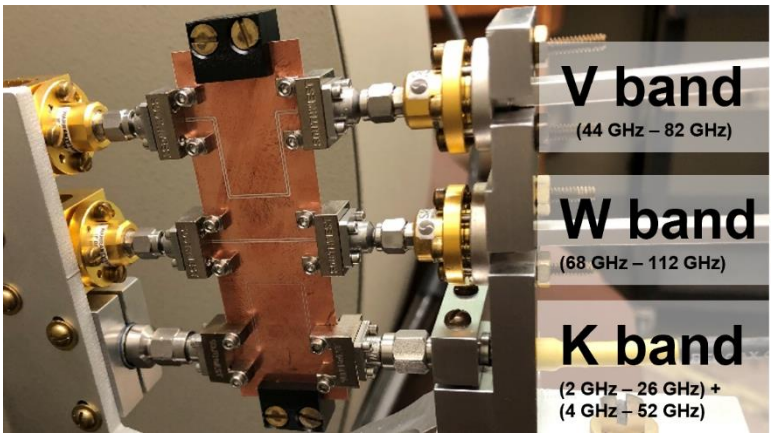

Figure 4: Connectorized probe showing the dedicated transmission lines for K, V, and W bands.

4. Mechanical and Magnetic Assembly

The GCPWG board is rigidly mounted to a custom-machined aluminum assembly cart that slides onto a track attached to the electromagnet.

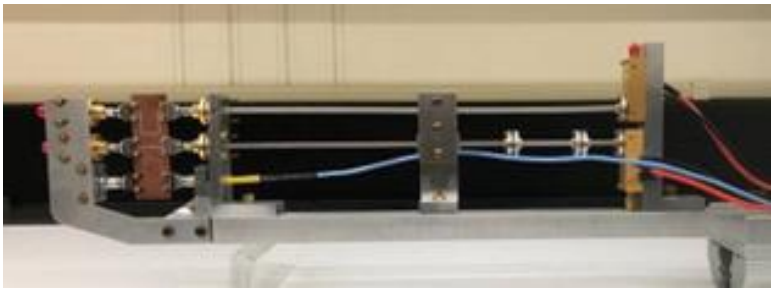

Figure 5: The complete transmission line assembly cart, compatible with a standard 2.5 T electromagnet sliding track.

4.1 Electromagnet and Modulation

- **Magnet:** A 150 mm diameter, 70 Amp dipole electromagnet with pole caps tapered to 25 mm diameter. With a gap of 25 mm, a maximum field 2.5 T is generated.
- **Field Modulation:** To enable lock-in detection, encapsulated Helmholtz coils are mounted directly around the GCPWG board. These are driven at 75 Hz with a peak amplitude of approximately 3 mT.

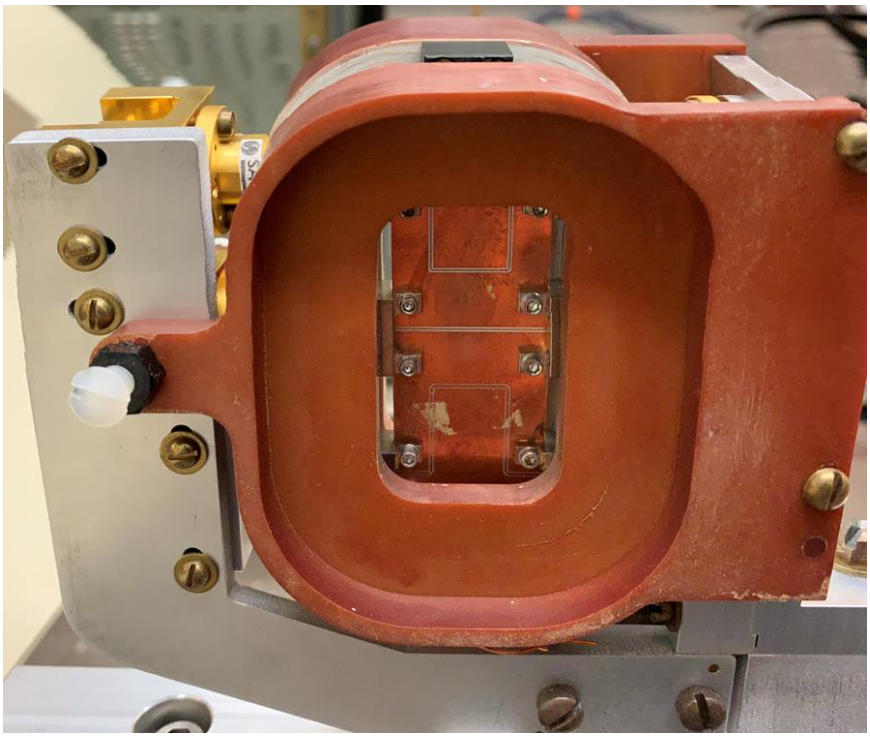

Figure 6: Encapsulated Helmholtz coils mounted around the GCPWG board to generate field modulation for lock-in detection.

5. Software and Automation

The system is automated using custom Python sequencing, utilizing open-source libraries to control laboratory instruments via GPIB, USB, and Serial ports.

- **Measurement Logic:** The software steps the magnetic field and holds it static. The lock-in amplifier is read after a settling time equal to three (3) time constants to ensure signal stability.
- **Real-Time Analysis:** A custom Python plotter visualizes the data as it is generated, performing real-time extraction of spectroscopic parameters.

6. Data Analysis and Fitting Algorithms

Because the system employs field modulation and lock-in detection, the measured signal represents the differential response to the AC magnetic field. Consequently, the data takes the form of the derivative of the absorption profile rather than a simple peak [6].

6.1 The Derivative Lorentzian Model

To accurately extract the resonance field (H_{res}) and linewidth (ΔH), the software fits the data to the derivative of a Lorentzian function. This model accounts for the phase-

insensitive nature of RF diode detection by including both absorptive (A) and dispersive (D) components:

$$\frac{dL}{dH} = A\frac{H - H_{res}}{[(H - H_{res})^2 + (\Delta H/2)^2]^2} + D\frac{(H - H_{res})^2 - (\Delta H/2)^2}{[(H - H_{res})^2 + (\Delta H/2)^2]^2}$$

Where:

- H is the applied field.
- H_{res} is the resonance field center.
- ΔH is the full-width at half-maximum (FWHM) linewidth.
- A and D are amplitude scaling factors for the absorptive and dispersive components, respectively.

6.2 Multi-Mode Fitting

For samples exhibiting Perpendicular Standing Spin Waves (PSSW), multiple resonances may appear in a single field sweep. The analysis software fits the total signal as the sum of individual derivative Lorentzian functions [7]:

$$\frac{dL_{tot}}{dH} = \sum_{i=1}^{n} \frac{dL\left(H, H_{res}^i, \Delta H^i; A^i, D^i\right)}{dH}.$$

This approach allows for the simultaneous extraction of the fundamental mode ($n = 0$) and higher-order spin-wave modes ($n = 1, 2$ ...), which is critical for determining the exchange stiffness.

7. Detection and Calibration

The system operates in absorption mode using diode detectors optimized for their respective bands.

- **Detectors:** Zero-bias Schottky diode detectors are used for signal rectification. While waveguide detectors (WR-15 and WR-10) are standard for V and W bands, coaxial 2.4 mm detectors have been successfully used interchangeably across the V-band (up to 75 GHz).
- **Field Calibration:** Because the Hall probe (Teslameter) is offset from the sample, a look-up table is generated using a DPPH reference sample and a calibrated CoFeB thin film reference sample to correlate the Teslameter reading to the actual field at the W, V, and K band positions.

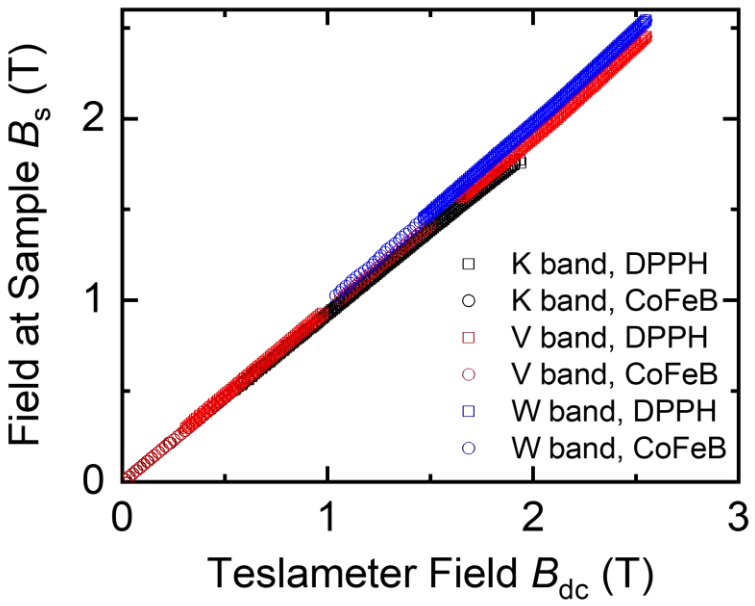

Figure 7: Field calibration curves correlating the Teslameter reading to the actual field at the sample location for all three bands.

8. Typical Performance and Data Quality

The primary advantage of this system is the ability to resolve fine spectral features at high frequencies that are typically obscured by noise in standard systems.

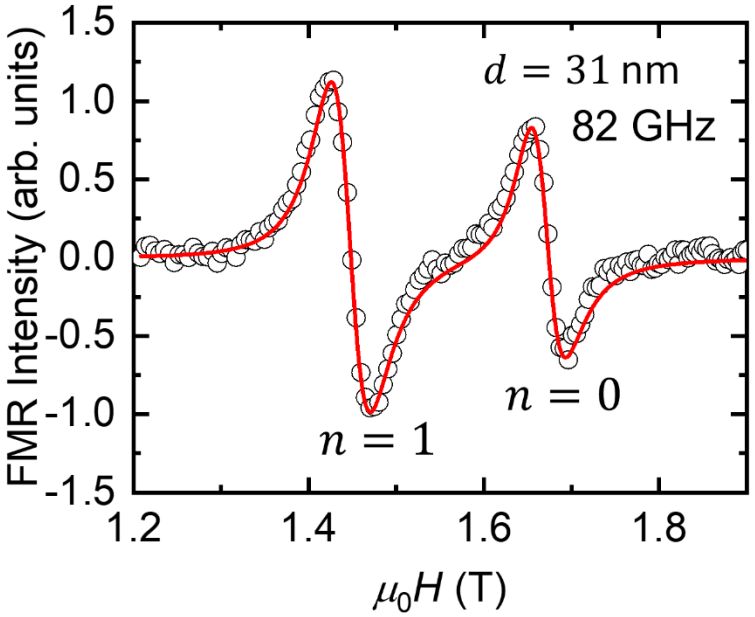

Figure 8: High-fidelity derivative absorption spectra at 82 GHz fitted using the derivative

Lorentzian model described in Section 7. Note the clear resolution between the fundamental ($n = 0$) and first perpendicular standing spin-wave ($n = 1$) modes, achieved using the custom GCPWG probe.

Furthermore, the system maintains high phase stability across the broad frequency spectrum, allowing for accurate extraction of linewidths (ΔH) well into the high-frequency bands. Figure 9 displays the linewidth evolution for a 23 nm Fe-Pd sample. The linearity of the fit confirms the system's sensitivity and baseline stability, enabling the precise extraction of a low Gilbert damping parameter ($\alpha \approx 0.007$) which would be difficult to quantify using lower-frequency datasets alone.

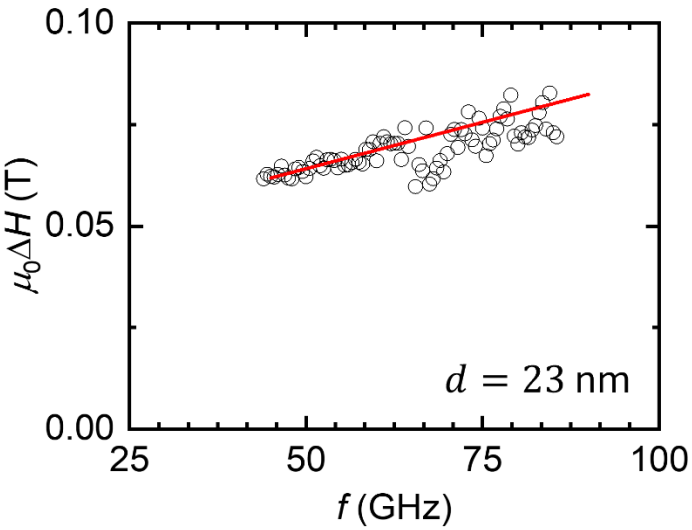

Figure 9: Frequency dependence of the linewidth (ΔH) measured on the 23-nm-thick $L1_0$ Fe-Pd sample. The data exhibits a clear linear dependence on frequency, consistent with Gilbert damping $\alpha \approx 0.007$. The ability to track linewidth evolution with a high signal-to-noise ratio into the V and W bands is critical for accurately separating extrinsic inhomogeneity (ΔH_0) from intrinsic damping (α).

9. Bill of Materials (BOM) & Key Specs

Component Category	**Part / Specification**	**Notes**
RF Board	Rogers 4350 Laminate [8]	0.20 mm thick, 0.025 mm Cu cladding.
RF Connectors	1.0 mm End-launch	For W-band. Pin diameter 0.13 mm.

Component Category	Part / Specification	Notes
RF Connectors	2.4 mm End-launch	For K-band. Pin diameter 0.18 mm.
Signal Source	Microwave Generators (x3)	2 GHz—26 GHz range, -20 dBm to 10 dBm output.
Multipliers	Active Multipliers (x2, x4, x6)	Delivering 16 dBm output power.
Detectors	Zero-Bias Diode Detectors	Coaxial (K-band) and Waveguide (V/W-band).
Magnetics	2.5 T Electromagnet	25 mm pole gap.
Modulation	Helmholtz Coils	75 Hz AC magnetic field, 3 mT amplitude.
Mechanical	Sliding Assembly Cart	Custom Machined Aluminum.

10. Conclusion

By combining commercial microwave components with a carefully engineered GCPWG board, robust Python automation, and rigorous derivative lineshape fitting, this 112 GHz spectrometer provides a high-fidelity window into the dynamics of high-anisotropy magnetic materials. This instrument is essential for researchers aiming to validate theoretical models of Heisenberg exchange and damping in the ultra-thin films that will power future MRAM technologies.

11. Acknowledgments

This work was performed with funding from the CHIPS Metrology Program, part of CHIPS for America, National Institute of Standards and Technology, U.S. Department of Commerce.

---

12. References

[1] D. Huang, J.E. Shoup, et al., "Competing explanations for spin-wave resonances in $L1_0(001)$ Fe-Pd thin films with perpendicular magnetic anisotropy," *Phys. Rev. Applied*, vol. 24, 064006, 2025.

[2] S. Klingler, A. V. Chumak, T. Mewes, B. Khodadadi, C. Mewes, C. Dubs, O. Surzhenko, B. Hillebrands, and A. Conca, "Measurements of the exchange stiffness of YIG films using broadband ferromagnetic resonance techniques," *J. Phys. D: Appl. Phys.*, vol. 48, p. 015001, 2015.
[3] C. Kittel, "Excitation of spin waves in a ferromagnet by a uniform rf field," *Phys. Rev.*, vol. 110, p. 1295, 1958.
[4] X. Wang, S. Krylyuk, D. Josell, D. Zhang, D. Lyu, J.-P. Wang, and D. B. Gopman, "Buffer layer engineering of $L1_0$-FePd thin films with large perpendicular magnetic anisotropy," *AIP Adv.*, vol. 11, p. 025106, 2021.
[5] Southwest Microwave, "Optimizing test boards for 50 GHz end launch connectors: grounded coplanar launches and through lines on 30 mil Rogers 4350 with comparison to microstrip," [Online]. Available: https://mpd.southwestmicrowave.com/wp-content/uploads/2018/07/Optimizing-Test-Boards-for-50-GHz-End-Launch-Connectors.pdf.
[6] D. B. Gopman, J. W. Lau, K. P. Mohanchandra, K. Wetzlar, and G. P. Carman, "Determination of the exchange constant of $Tb_{0.3}Dy_{0.7}Fe_2$ by broadband ferromagnetic resonance spectroscopy," *Phys. Rev. B*, vol. 93, p. 064425, 2016.
[7] D. B. Gopman, V. Sampath, H. Ahmad, S. Bandyopadhyay, and J. Atulasimha, "Static and dynamic magnetic properties of sputtered Fe-Ga thin films," *IEEE Trans. Magn.*, vol. 53, p. 1, 2017.
[8] Certain equipment, instruments, software, or materials are identified in this paper in order to specify the experimental procedure adequately. Such identification is not intended to imply recommendation or endorsement of any product or service by NIST, nor is it intended to imply that the materials or equipment identified are necessarily the best available for the purpose.